Bandwidth-on-Demand Motion Control

S.J.L.M. van Loon, B.G.B. Hunnekens, A.S. Simon, N. van de Wouw, and W.P.M.H. Heemels

***Abstract*— In this brief, we introduce a "bandwidth-on-demand" variable-gain control (VGC) strategy that allows for a varying bandwidth of the feedback controller. The proposed VGC can achieve improved performance given time-varying, reference-dependent performance requirements compared with linear time-invariant (LTI) control suffering from design tradeoffs between low-frequency tracking performance and sensitivity to higher-frequency disturbances. The VGC consists of frequency-domain loop-shaped linear filters and a variable-gain element, which depends on reference information. We present easy-to-use controller design guidelines and data-based frequency-domain conditions to verify stability and convergence of the closed-loop system. Moreover, the ability of the "bandwidth-on-demand" controller to outperform LTI controllers is emphasized through experiments on an industrial nanopositioning motion stage.**

***Index Terms*— Control design tradeoffs, frequency-domain, industrial application, motion control, variable-gain control (VGC).**

I. Introduction

THE increasing performance demands on speed, accuracy, throughput, and soon, of today's high-precision motion systems require them to operate under diverse modes of operation, each having their own specific set of performance requirements. If this comes with the presence of multiple disturbance sources, active in various frequency ranges, this poses a challenging control design task. This is due to the fact that the vast majority of controller designs techniques generally rely on classical linear control theory in which fundamental design tradeoffs are inherently present. Namely, increasing the bandwidth of the controlled system improves the low-frequency disturbance rejection properties, and, hence, the tracking performance, but due to the waterbed effect, this also results in a larger sensitivity to higher-frequency disturbances (i.e., around and/or above the bandwidth) [1]. This fundamental tradeoff can already be challenging when just one mode of operation is considered, but this is severely aggravated when high performance is required in multiple modes of operation, because this generally means that the control objectives vary over time, e.g., depend on the reference. As an example, we like to comment on the conflicting control design situation that arises for typical third/fourth-order reference profiles used in many industrial positioning systems, such as pick-and-place machinery, metrology stages, lithographic systems, copiers, and so on. During standstill, high-frequency disturbance sources are often dominant over low-frequency disturbance sources, such that a low bandwidth (LBW) of the controlled system is desired in order not to amplify these high-frequency disturbances. On the other hand, when the reference is changing low-frequency disturbances play a dominant role in the closed-loop error, and, hence, a high bandwidth (HBW) is preferred to achieve good tracking performance. Due to fundamental limitations in linear time-invariant (LTI) feedback control, the design of one LTI controller typically requires a compromise between these conflicting design goals thereby limiting the overall performance achievements of the controlled system. This problem generically arises in motion applications, but is also relevant for entirely different applications such as the control of dimmers for lighting applications in which a tradeoff between the sensitivity to the time-varying reference induced by a user turning the dimmer knob and the sensitivity to high-frequency, e.g., net-induced, disturbances also arises naturally.

In this brief, we propose a variable-gain control (VGC) strategy that allows for a reference-dependent, and thus time-varying, "bandwidth" of the feedback controller. By taking online reference information into account, this feature allows to "anticipate" on the "required bandwidth" for each mode of operation. This allows, contrary to LTI control, to deal with the conflicting control objectives induced by reference-dependent dominance of multiple disturbance sources that are acting in various frequency ranges. The proposed controller consists of frequency-domain loop-shaped linear filters and a variable-gain element, with its gain depending on reference information and inducing the desired "bandwidth" of the resulting controller. The proposed controller structure supports the design of all the linear components of the VGC configuration using well-known (frequency-domain) loop-shaping techniques [2]. It therefore connects to the state-of-the-art industrial motion control setting, in which easy-to-measure frequency response functions (FRFs) play an important role in the controller design, e.g., by using frequency-domain loop-shaping techniques.

The concept of VGC has already been successfully applied in numerous industrial applications to improve the performance of (linear) motion systems [3]–[7]. In fact, the use of VGC to target similar LTI control design tradeoffs as considered in this brief, i.e., balancing tradeoffs

Manuscript received June 29, 2016; revised January 8, 2017; accepted January 17, 2017. Date of publication February 7, 2017; date of current version December 14, 2017. Manuscript received in final form January 22, 2017. Recommended by Associate Editor G. Cherubini. This work was supported by the Dutch Technology Foundation (STW) through the Project HyperMotion: Hybrid Control for Performance Improvement of Linear Motion Systems under Project 10953.

S.J.L.M. van Loon, B.G.B. Hunnekens, A.S. Simon, and W.P.M.H. Heemels are with the Department of Mechanical Engineering, Eindhoven University of Technology, 5600 MB Eindhoven, The Netherlands (e-mail: s.j.l.m.v.loon@tue.nl; b.g.b.hunnekens@tue.nl; a.s.simon@tue.nl; m.heemels@tue.nl).

N. van de Wouw is with the Department of Mechanical Engineering, Eindhoven University of Technology, 5600 MB Eindhoven, The Netherlands, also with the Department of Civil, Environmental and Geo-Engineering, University of Minnesota, Minneapolis, MN 55455 USA, and also with the Delft Center for Systems and Control, Delft University of Technology, 2628 CD Delft, The Netherlands (e-mail: n.v.d.wouw@tue.nl).

Color versions of one or more of the figures in this paper are available online at http://ieeexplore.ieee.org.

Digital Object Identifier 10.1109/TCST.2017.2658192

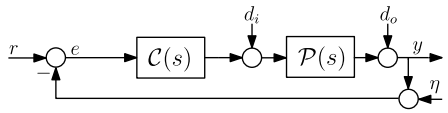

Fig. 1. Schematic representation of a classical LTI feedback controlled system.

between low-frequency tracking properties and sensitivity to higher-frequency disturbances, has been considered in [5] and [6]. The novelty in our approach lies in the fact that we couple this fundamental tradeoff to time-varying control objectives depending on online reference information, which makes it possible to design a time-varying controller with a "bandwidth-on-demand" characteristic.

Other techniques that can deal with the considered tradeoff are, e.g., linear parameter-varying (LPV) control [8]–[10] and switched controller design [11], [12]. The main drawback of these approaches, compared with the control design proposed in this brief, is that they require accurate parametric plant models and solving linear matrix inequalities for design [12], [13], which both are less desirable from a practical point of view.

The main contributions of this brief are as follows. First, a novel reference-dependent VGC strategy is introduced that has a "bandwidth-on-demand" characteristic and is applicable to generic (motion) control problems. Second, easy-to-use design guidelines are presented as well as graphical data-based conditions to verify stability and convergence of the variable-gain controlled closed-loop system. Third, the entire design process and its potential to outperform LTI controllers are experimentally demonstrated on an industrial case study of a nanopositioning motion stage.

A. Nomenclature

Let $\mathbb{C}$ and $\mathbb{R}$ denote the set of complex and real numbers, respectively. The real part of a complex variable z is denoted by $Re(z)$. The Laplace transform of a signal $x : \mathbb{R}_{\geq 0} \to \mathbb{R}^n$ is denoted by $\mathfrak{L}\{x\}$ and $s \in \mathbb{C}$ denotes the Laplace variable. Consider the LTI feedback control configuration in Fig. 1 with single-input–single-output (SISO) LTI plant $\mathcal{P}(s)$, $s \in \mathbb{C}$, and an SISO LTI controller $\mathcal{C}(s)$. The bandwidth ω_b is defined as the frequency $\omega \in \mathbb{R}$ where the magnitude of the open-loop $|\mathcal{P}(j\omega)\mathcal{C}(j\omega)|$ crosses 1 from above for the first time [14].

II. Reference-Dependent VGC

In this section, a reference-dependent VGC strategy with a "bandwidth-on-demand" characteristic will be proposed, which allows for a reference-dependent "bandwidth" of the feedback controller, i.e., the "bandwidth" (and thereby the controller) is varied online based on a relation between the preferred bandwidth and the actual reference characteristics.

Remark 1: By definition, bandwidth is an LTI concept and, hence, does not apply to our proposed time-varying control strategy. Nevertheless, with some abuse of definition, we will use the term "bandwidth" in this brief but use quotation marks to avoid confusion with the LTI case.

The overall reference-dependent feedback control configuration as proposed in this brief is shown in Fig. 2. It consists of a standard LTI feedback controlled system, similar to Fig. 1 with $\mathcal{C}(s) = \mathcal{C}_{\text{lbw}}(s)$, augmented with an add-on VGC part.

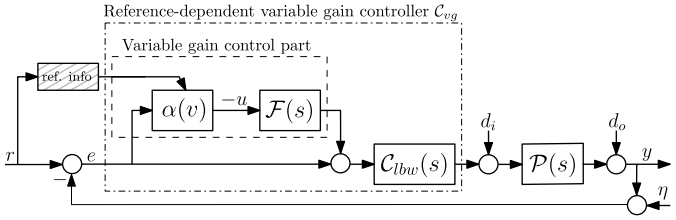

Fig. 2. Schematic representation of the reference-dependent VGC system.

Moreover, in Fig. 1, d_i and d_o denote unknown, bounded input/output disturbances, respectively, and $e := r - y - \eta$ denotes the tracking error between the reference signal r, the output y of $\mathcal{P}(s)$, $s \in \mathbb{C}$, and the measurement noise η. The variable gain part of the total controller $\mathcal{C}_{\text{vg}}$ consists of an LTI shaping filter $\mathcal{F}(s)$, and a time-varying variable gain $\alpha(v(t))$ depending on a *scheduling variable* $v(t)$, $t \in \mathbb{R}_{\geq 0}$, which is related to characteristics of the reference signal. In this brief, and in particular in Section IV, we will use the reference velocity as scheduling variable, i.e., $v(t) = \dot{r}(t)$, although other options are imaginable as well. For instance, the variable gain could depend on the reference position, i.e., $v(t) = r(t)$, on the acceleration, i.e., $v(t) = \ddot{r}(t)$, or combinations and so on. The process of extracting the relevant information, e.g., $v(t) = \dot{r}(t)$, from the reference signal r is indicated by the dashed box in Fig. 2. Note that for the particular choices mentioned, the reference information is not required to be known in advance. The variable gain element is given by a mapping $\alpha : \mathbb{R} \to [0, \bar{\alpha}]$, where $\bar{\alpha} \in \mathbb{R}_{>0}$ denotes the maximum value. Let us first consider the situation where $\alpha \in [0, \bar{\alpha}]$ is a *fixed* gain, and study the following cases ($\alpha = 0$ and $\alpha \in (0, \bar{\alpha}]$).

1) If $\alpha = 0$, we have a linear control scheme with linear controller $\mathcal{C}_{\text{vg}}^f(s) = \mathcal{C}_{\text{lbw}}(s)$.
2) For a *fixed* $\alpha \in (0, \bar{\alpha}]$, we have a linear control scheme with controller

$$\mathcal{C}_{\text{vg}}^f(s) = (1 + \alpha\mathcal{F}(s))\mathcal{C}_{\text{lbw}}(s). \tag{1}$$

Remark 2: The reference-dependent VGC reduces only to an LTI controller for fixed values of α. Therefore, we denote it by $\mathcal{C}_{\text{vg}}^f(s)$ only when α is *fixed*, and use $\mathcal{C}_{\text{vg}}$ with $\alpha(v(t))$ varying over time otherwise.

This variable gain allows us to deal with the conflicting design criteria as described in Section I, i.e., preferring a controller that results in a LBW $\underline{\omega}_b$ over a controller that results in a higher bandwidth $\underline{\omega}_b < \omega_b \leq \overline{\omega}_b$, or vice versa, *depending on actual reference information*. Here, $\overline{\omega}_b$ denotes the highest bandwidth that we consider. In fact, by assigning $\alpha(v(t)) = 0$ to the situation where a LBW is preferable, the user can loop-shape the controller $\mathcal{C}_{\text{lbw}}(s)$ such that the best possible performance is obtained for this particular situation. On the other hand, the proposed structure of the reference-dependent VGC $\mathcal{C}_{\text{vg}}$ allows that, by proper design of the variable-gain element $\alpha : \mathbb{R} \to [0, \bar{\alpha}]$ and the linear filter $\mathcal{F}(s)$ (see in Section III-B), the "bandwidth" ω_b of the VGC $\mathcal{C}_{\text{vg}}^f(s)$ (for fixed values of α) will gradually increase (and can take values in $[\underline{\omega}_b, \overline{\omega}_b]$) for increasing values of $\alpha \in [0, \bar{\alpha}]$.

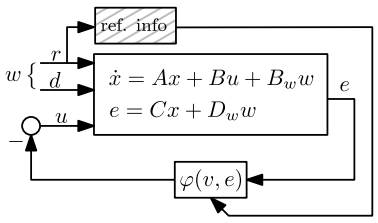

Fig. 3. Schematic representation of a Lur'e-type description of the reference-dependent VGC system.

III. Stability Conditions and Design Guidelines

In Section III-A, we present data-based graphical conditions to verify stability and convergence ([15], [16]) of the closed-loop system as in Fig. 2 for every mapping $\alpha : \mathbb{R} \to [0, \bar{\alpha}]$ and any choice of scheduling variable v (even when v is discontinuous). Moreover, general design guidelines are provided in Section III-B.

A. Stability and Convergence

The system, as in Fig. 2, belongs to the class of Lur'e-type systems [17], as depicted schematically in Fig. 3. Such systems consist of a linear dynamical part in feedback with a time-varying, but memoryless, variable-gain element given (in this case) by $\varphi(v(t), e)$. Consider therefore Fig. 3, in which the linear part is given by

$$\mathfrak{L}\{e\} = \mathcal{G}_{\text{eu}}(s)\mathfrak{L}\{u\} + \mathcal{G}_{\text{ew}}(s)\mathfrak{L}\{w\} \tag{2}$$

in which the external inputs are denoted by $w = [r\ d^\top]^\top \in \mathbb{R}^{n_w}$, and the vector $d = [d_i^\top\ \ d_o^\top\ \ \eta]^\top \in \mathbb{R}^{n_d}$ contains the external disturbances. In (2), the transfer function between "input" u and "output" e (see Fig. 3) is given by

$$\mathcal{G}_{\text{eu}}(s) = \mathcal{F}(s)\underbrace{\frac{\mathcal{P}(s)\mathcal{C}_{\text{lbw}}(s)}{1 + \mathcal{P}(s)\mathcal{C}_{\text{lbw}}(s)}}_{=:\mathcal{T}(s)} \tag{3}$$

in which $\mathcal{T}(s)$ represents the complementary sensitivity function, and the transfer function between the external inputs w and e is given by $\mathcal{G}_{\text{ew}}(s) = \begin{bmatrix}\mathcal{S}(s) & -\mathcal{S}_p(s) & -\mathcal{S}(s) & -\mathcal{S}(s)\end{bmatrix}$, in which $\mathcal{S}(s)$ and $\mathcal{S}_p(s)$ represent the sensitivity and process sensitivity function, respectively. The closed-loop dynamics can be represented in state-space form as

$$\dot{x} = Ax + Bu + B_w w \tag{4a}$$

$$e = Cx + D_w w, \quad u = -\varphi(v, e) \tag{4b}$$

with state $x \in \mathbb{R}^{n_x}$, (A, B, C) minimal such that $\mathcal{G}_{\text{eu}}(s) = C(sI - A)^{-1}B$, and $\mathcal{G}_{\text{ew}}(s) = C(sI - A)^{-1}B_w + D_w$ with I an identity matrix of appropriate dimensions. Finally, the variable-gain in Fig. 3 depends on the reference via

$$\varphi(v, e) = \alpha(v)e, \quad \text{for all } v \in \mathbb{R} \text{ and } e \in \mathbb{R}. \tag{5}$$

If (the origin of the) the system (4) and (5) is asymptotically stable for a *fixed* value of α (in the absence of external disturbances, i.e., $w = 0$), it is known (via linear system theory) that it exhibits a unique, bounded, and globally asymptotically stable steady-state solution (irrespective of the initial condition) for any bounded signals of external variables [18]. Clearly, such a property does not hold in general for nonlinear systems such as the closed-loop system with the *variable-gain* as studied here. However, here we establish conditions such that these favorable properties can be guaranteed also for systems with time-varying gains $\alpha(v(t))$, independent of the particular reference r (recall that $v(t) = \dot{r}(t)$). In the literature, such a property is called convergence (see [15], [16]). Before we provide conditions to ensure that our proposed VGC design renders the closed-loop system (4), (5) convergent, we first provide a formal definition of a convergent system. Therefore, consider a general nonlinear system description of the form

$$\dot{x} = f(x, w, t) \tag{6}$$

with state $x \in \mathbb{R}^{n_x}$ and input $w \in \mathbb{R}^{n_w}$. The function $f(x, w, t)$ is locally Lipschitz in x, continuous in w, and piecewise continuous in t. Moreover, the inputs w are assumed to be piecewise continuous functions of time defined for all times $t \in \mathbb{R}$.

Definition 3 [15], [16]: System (6) is said to hold the following.

1) *convergent* if there exists a solution $\bar{x}_w(t)$ such that the following hold.
   a) $\bar{x}_w(t)$ is defined and bounded for all $t \in \mathbb{R}$.
   b) $\bar{x}_w(t)$ is globally asymptotically stable.
2) *exponentially convergent* if it is convergent and $\bar{x}_w(t)$ is globally exponentially stable.

In Definition 3, the solution $\bar{x}_w(t)$ [which depends on the input $w(t)$] denotes the steady-state solution of the system (6). Exponential convergence implies first, exponential stability for any reference and disturbance realization, and second, the existence of a unique steady-state solution [16]. The latter property allows for a unique steady-state performance evaluation in the face of disturbances, and, as such, it also results in an easier design and tuning of the VGC $\mathcal{C}_{\text{vg}}$. The following conditions are sufficient to establish that a system of the form (4) and (5) is exponentially convergent.

Theorem 4: Consider system (4) with variable-gain $\varphi(v, e)$ given by (5), in which $\alpha : \mathbb{R} \to [0, \bar{\alpha}]$ for all $t \in \mathbb{R}$ for some $\bar{\alpha} \in \mathbb{R}_{>0}$. Suppose that the following hold. (I)

1) The system matrix A is Hurwitz.
2) $\mathcal{G}_{\text{eu}}(j\omega)$ as in (3) satisfies

$$\frac{1}{\bar{\alpha}} + \text{Re}(\lim_{\omega \to \infty} \mathcal{G}_{\text{eu}}(j\omega)) > 0 \tag{7}$$

and

$$\frac{1}{\bar{\alpha}} + \text{Re}(\mathcal{G}_{\text{eu}}(j\omega)) > 0 \quad \text{for all} \quad \omega \in \mathbb{R}. \tag{8}$$

Then, system (4) and (5) is exponentially convergent.

Proof: The proof basically follows the reasoning of the proof in [5], [16], and [19], with the minor difference that in our system $\varphi(v, e)$ as in (5) depends on the scheduling variable $v(t)$, $t \in \mathbb{R}$. We note that a key step of the proof of [5], [16], and [19] consists of proving incremental stability, i.e., showing that two solutions $x_1 : \mathbb{R} \to \mathbb{R}^{n_x}$ and $x_2 : \mathbb{R} \to \mathbb{R}^{n_x}$ subject to the same scheduling variable v and external inputs d, but with different initial conditions, converge to each other. It is essential for this part of the proof to observe

that $\alpha(v(t))$, $t \in \mathbb{R}$, is exactly the same for both solutions given the external inputs (including r and thus v). □

Remark 5: Condition (I) of Theorem 4 will be satisfied by proper controller design of $\mathcal{C}_{\text{lbw}}(s)$. This is due to the fact that if the open-loop $\mathcal{P}(s)\mathcal{C}_{\text{lbw}}(s)$ satisfies the Nyquist stability criterion [14], the complementary sensitivity function $\mathcal{T}(s)$ has all its poles located in the complex left half plane (LHP). In addition, if the shaping filter $\mathcal{F}(s)$ is designed such that it has no unstable poles, the transfer function $\mathcal{G}_{\text{eu}}(s)$ as in (3) will have all its poles located in the LHP as well. As a result, the system matrix A of (4) will be a Hurwitz matrix. Moreover, note that for many motion systems $\mathcal{G}_{\text{eu}}(j\omega) \to 0$ for $\omega \to \infty$, resulting in condition (7) being satisfied automatically.

B. Design and Tuning Guidelines

In this section, we present a four-step systematic design approach of a reference-dependent VGC $\mathcal{C}_{\text{vg}}$ as in Fig. 2, where we assume that a plant model $\mathcal{P}(s)$ is available, e.g., identified based on measured frequency response data.

Step 1 (Study the Control Tradeoff): The first step consists of studying the control design tradeoff in greater detail, which can be done in a model-based environment as well as by means of experiments. The following knowledge is required to perform this study:

1) The minimum and maximum scheduling variable under which the system needs to operate, i.e., determine $\underline{v}$ and $\overline{v}$ such that $v(t) \in [\underline{v}, \overline{v}]$ for all $t \in \mathbb{R}_{\geq 0}$;
2) A performance measure $J(v, \omega_b)$ depending on the scheduling variable v and the bandwidth ω_b, typically related to the application at hand (in this brief, we assume that a low J corresponds to a good performance);
3) *Model-Based Study:* A (rough) estimation of the types, and corresponding frequency ranges, of the disturbances acting on the system, i.e., d_i, d_o, and η in Fig. 1.

Consider the model structure as in Fig. 1 in which (in the case of a model-based study) we use the estimated plant model $\mathcal{P}(s)$. First, we define a grid of constant scheduling variables $v_{c,i}$, $i = 1, 2, \ldots, n$, satisfying $v_{c,i} \in [\underline{v}, \overline{v}]$ with $\underline{v} = v_{c,1} < v_{c,2} < \cdots < v_{c,n-1} < v_{c,n} = \overline{v}$. Moreover, we design m LTI controllers $\mathcal{C}_j(s)$ (see Fig. 1) with each a different bandwidth $\omega_{b,j}$, $j = 1, 2, \ldots, m$. Then, for *each* of these constant scheduling variables $v_{c,i}$, $i = 1, 2, \ldots, n$, we evaluate the performance for *each* of these LTI controllers $\mathcal{C}_j(s)$, $j = 1, 2, \ldots, m$. This allows us to (approximately) characterize the performance as a function of the bandwidth for each $v_{c,i}$, $i = 1, 2, \ldots, n$. This results in "performance" curves as schematically shown in Fig. 4. Fig. 4 represents the control design tradeoff, because each particular value $v_{c,i}$ for the scheduling variable will typically show optimal performance (minima in Fig. 4, indicated by the black dots) for a different bandwidth ω_b. We denote this "optimal bandwidth" by $\omega_{b,\text{opt},i}$ for the corresponding scheduling variable $v_{c,i}$, and is given by

$$\omega_{b,\text{opt},i} = \arg\min_{\omega_b} J(v_{c,i}, \omega_b), \quad \text{for } i = 1, 2, \ldots, n. \tag{9}$$

Step 2 (Design of a Low-Bandwidth and High-Bandwidth Controller $\mathcal{C}_{\text{lbw}}(s)$ and $\mathcal{C}_{\text{hbw}}(s)$, Respectively): Based on

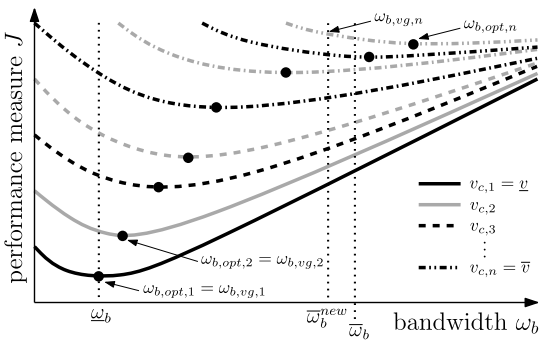

Fig. 4. Schematic representation of a control design tradeoff for a range of constant scheduling variables $v_{c,i} \in [\underline{v}, \overline{v}]$, $i = 1, 2 \ldots, n$, with $v_{c,1} = \underline{v}$ and $v_{c,n} = \overline{v}$.

Step 1, we select the desired LBW $\underline{\omega}_b$ as $\underline{\omega}_b = \min_{i=1,2,\ldots,n} \omega_{b,\text{opt},i}$, and take $\mathcal{C}_{\text{lbw}}(s)$ as the corresponding LTI controller. In **Step 4**, we will ensure that the VGC $\mathcal{C}_{\text{vg}}^f(s)$ represents $\mathcal{C}_{\text{lbw}}(s)$ if $\alpha(\underline{v}) = 0$. The LTI controller $\mathcal{C}_{\text{hbw}}(s)$ is designed[1] such that the highest achievable bandwidth $\overline{\omega}_b$ is obtained under sufficient robustness margins,[2] such as gain margin, modulus margin, phase margin, and so on [14]. This HBW controller $\mathcal{C}_{\text{hbw}}(s)$ is the "target" controller for the high-gain situation, i.e., when $\alpha(\overline{v}) = \bar{\alpha}$, we aim to approximate $\mathcal{C}_{\text{hbw}}(s)$ with our VGC $\mathcal{C}_{\text{vg}}^f(s)$. How to achieve this will be discussed in the next step.

Step 3 (Design the Linear Filter $\mathcal{F}(s)$ and Determine the Maximum Allowable Gain $\bar{\alpha}$): In this step, we design $\mathcal{F}(s)$ and $\bar{\alpha}$ with the aim to vary the "bandwidth" ω_b of the resulting controller $\mathcal{C}_{\text{vg}}$ online in the set $[\underline{\omega}_b, \overline{\omega}_b]$, depending on the scheduling variables v. The control architecture of the proposed VGC as in Fig. 2 results in $\mathcal{C}_{\text{vg}}^f(s) = \mathcal{C}_{\text{lbw}}(s)$ for the limit case $\alpha = 0$, as already mentioned. For the other limit case, $\alpha = \bar{\alpha}$, we aim to design $\mathcal{F}(s)$, and determine $\bar{\alpha}$, such that

$$(1 + \bar{\alpha}\mathcal{F}(s))\mathcal{C}_{\text{lbw}}(s) = \mathcal{C}_{\text{hbw}}(s). \tag{10}$$

When satisfying (10) *exactly*, we obtain values of $\bar{\alpha}$ and $\mathcal{F}(s)$ (which is normalized to gain 1 when $j\omega = 0$) corresponding to an "optimal high-gain situation," satisfying

$$\bar{\alpha}_{\text{opt}}\mathcal{F}_{\text{opt}}(s) = \frac{\mathcal{C}_{\text{hbw}}(s)}{\mathcal{C}_{\text{lbw}}(s)} - 1. \tag{11}$$

From (11) and the normalization $\mathcal{F}_{\text{opt}}(j\omega) = 1$ when $j\omega = 0$, $\bar{\alpha}_{\text{opt}}$ and $\mathcal{F}_{\text{opt}}(s)$ can be determined uniquely. However, this optimal choice might not always be practically feasible due to the following reasons.

1) This approach does *not* guarantee *a priori* the closed-loop stability of (4) and (5), for the obtained $\bar{\alpha}_{\text{opt}}$ and $\mathcal{F}_{\text{opt}}(s)$;
2) This approach of fixing $\bar{\alpha}$ and $\mathcal{F}(s)$ leaves the designer with no possibilities to influence the shape of $\mathcal{G}_{\text{eu}}(j\omega)$ as in (3), e.g., through the manual shaping of $\mathcal{F}(s)$,

[1]Note that both $\mathcal{C}_{\text{lbw}}(s)$ and $\mathcal{C}_{\text{hbw}}(s)$ can be designed using well-known frequency-domain loop-shaping techniques [2].

[2]In this respect, note that (in general) $\overline{\omega}_b \neq \max_{i=1,2,\ldots,n} \omega_{b,\text{opt},i}$.

in order to satisfy the circle criterion condition (8) leading to stability and convergence guarantees [5].

3) For a large difference between $\underline{\omega}_b$ and $\overline{\omega}_b$, this approach might yield a high gain $\bar{\alpha}_{\text{opt}}$. Consequently, for such high values of $\bar{\alpha}_{\text{opt}}$, we have that $(1/(\bar{\alpha}_{\text{opt}})) \to 0$. Therefore, in such cases, the FRF $\mathcal{G}_{\text{eu}}(j\omega)$ as in (3), with $\bar{\alpha} = \bar{\alpha}_{\text{opt}}$ and $\mathcal{F}(s) = \mathcal{F}_{\text{opt}}(s)$, is required to be (almost) positive real in order to satisfy the conditions of Theorem 4, which in many (motion control) cases is a too strict requirement.

Therefore, it is often better to design the filter $\mathcal{F}(s)$ manually by loop-shaping techniques, in which $\mathcal{F}_{\text{opt}}(s)$ resulting from (11) can be used as a target design. In this respect, if (10) is not exactly satisfied for the resulting $\mathcal{F}(s)$ and $\bar{\alpha}$, the target bandwidth $\overline{\omega}_b$ can most probably not exactly be attained anymore. Therefore, from this point onward, the bandwidth of the resulting controller $\mathcal{C}_{\text{vg}}^f(s) = (1+\bar{\alpha}\mathcal{F}(s))\mathcal{C}_{\text{lbw}}(s)$ is denoted by $\overline{\omega}_b^{new}$, for which it typically holds that $\overline{\omega}_b^{new} \leq \overline{\omega}_b$. How to apply this step will be demonstrated in Section IV-B.

Step 4 (Design the "Reference-to-Gain" Mapping): The last step in the design of a reference-dependent VGC $\mathcal{C}_{\text{vg}}$ is to design the mapping $\alpha : [\underline{v}, \overline{v}] \to [0, \bar{\alpha}]$. We start by establishing a relation between the "bandwidth" ω_b of $\mathcal{C}_{\text{vg}}$ as a function of $\alpha \in [0, \bar{\alpha}]$. Note that, for fixed values of α, the controller $\mathcal{C}_{\text{vg}}^f(s)$ as in (1) (in which the shaping filter $\mathcal{F}(s)$ and maximal gain $\bar{\alpha}$ follow from **Step 3**) is linear and that the resulting bandwidth can be straightforwardly assessed. In particular, for each $\alpha_i \in [0, \bar{\alpha}]$, $i = 1, 2, \ldots, k$, on a discrete grid, we assess the corresponding bandwidth $\omega_{b,i}$, $i = 1, 2, \ldots, k$. By interpolation, the relation $\omega_b = H_{bw}(\alpha)$ can be approximately determined for all $\alpha \in [0, \bar{\alpha}]$. Here, we assume for simplicity that the map $H_{bw} : [0, \bar{\alpha}] \to [\underline{\omega}_b, \overline{\omega}_b^{new}]$ is strictly monotone (although one can also deal with other situations). Then, the desired "reference-to-gain" mapping $\alpha : [\underline{v}, \overline{v}] \to [0, \bar{\alpha}]$ is given by $\alpha(v) = \arg\min_{0 \leq \alpha \leq \bar{\alpha}} J(v, H_{bw}(\alpha))$. We want to emphasize that this step will never jeopardize stability and convergence of the system (4) and (5) as long as $\alpha(v(t)) \in [0, \bar{\alpha}]$, $t \in \mathbb{R}_{\geq 0}$ due to the stability and convergence guarantees obtained in **Step 3**.

Remark 6: The proposed "bandwidth-on-demand" controller offers more design freedom compared with a "standard" LTI controller to accommodate for reference-dependent performance requirements in the presence of multiple disturbance sources. Although its design process is slightly more involved, only well-known frequency-domain loop-shaping techniques are needed to design a "bandwidth-on-demand" controller following the four steps discussed in this section.

IV. Case Study on an Industrial Nanopositioning Motion Stage

The nanopositioning motion stage considered in this brief is an experimental setup of a high-precision motion stage that requires movements with velocities ranging from standstill, to nanometers per second, to even millimeters per second, all with (sub)nanometer resolution. The nanopositioning motion stage has several key modes of operation, namely: 1) standstill; 2) constant velocities in a broad range; and 3) fast (user-operated) point-to-point movements. Due to the presence of multiple disturbance sources in various frequency ranges (depending also on the mode of operation), this results in conflicting control design tradeoffs. As such, this nanopositioning motion stage forms a relevant case study to validate the practical feasibility of the proposed "bandwidth-on-demand" VGC strategy. An overview on the control for nanopositioning systems can be found in [20]. Here, we present the experimental study as a representative motion control problem for the new bandwidth-on-demand control methodology as presented in this brief. Note that this novel control design methodology is relevant for many other control applications as already discussed in Section I. The sole objective of the particular experimental nanopositioning study is to illustrate the design procedure, which can also be applied to many other problems. As such, a comparison with alternative control solutions for the nanopositioning stage is beyond the scope of this brief. As such, we refrain from a comparison with alternative control strategies for the particular application of nanopositioning.

Remark 7: To protect the interests of the manufacturer, we cannot provide concrete information about the reference velocities (and thus scheduling variables v) and the disturbance modeling. For the same reason, all figures in this section have either been scaled or use blank axes in terms of units.

A. Nanopositioning Motion Stage

The nanopositioning motion stage is driven by piezoelectric actuators, positioned on a vibration isolation table, and equipped with a first-order 100-Hz low-pass actuation filter $\mathcal{P}_{\text{act}}(s)$ in the hardware to filter off high-frequency actuator noise, given by the transfer function $\mathcal{P}_{\text{act}}(s) = 1/(1/(2\pi 100)s + 1)$. The plant $\mathcal{P}_n(j\omega)$ is identified based on measured FRFs with and without the additional low-pass filter, i.e., $\mathcal{P}_n(j\omega)\mathcal{P}_{\text{act}}(j\omega)$ and $\mathcal{P}_n(j\omega)$, respectively. This revealed, first, that the plant $\mathcal{P}_n(j\omega)$ behaves as a rigid-body system in the frequency range of interest (i.e., $\mathcal{P}_n(s) \approx 1/(ms^2)$ with mass m), and second, the presence of a significant, and thus bandwidth-limiting, delay.

The experimental nanopositioning motion setup operates in a laboratory environment instead of in its dedicated application. Therefore, additional disturbances are emulated to recover the real situation in the application as much as possible. Based on measurement data, an output disturbance $d_{o,\text{add}} = \mathcal{H}(s)\varepsilon$ has been identified, where the magnitude of $\mathcal{H}(j\omega)$ is depicted in Fig. 5 and ε is normally distributed white noise with zero mean and variance $\lambda_\varepsilon^2 = (2 \cdot 10^{-9})^2$. As a result, a controlled experiment is created that allows us to analyze the influence of the bandwidth ω_b on the performance measure as realistically as possible.

B. Design of a Reference-Dependent VGC

To illustrate the intuitive design of a reference-dependent VGC, we follow the design process using the guidelines presented in Section III-B, in which, from this point onward, the scheduling variable is taken as the reference velocity, i.e., $v(t) = \dot{r}(t)$, $t \in \mathbb{R}_{\geq 0}$.

Step 1 in the Design: In this step, we study the control design tradeoff in a model-based environment.

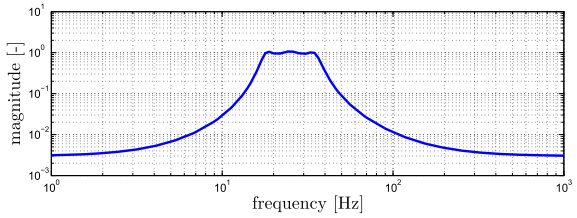

Fig. 5. Bode magnitude plot of the disturbance filter $\mathcal{H}(j\omega)$.

Consider therefore Fig. 1, in which the plant is given by $\mathcal{P}(s) = \mathcal{P}_n(s)\mathcal{P}_{\text{act}}(s)$, with $\mathcal{P}_n(s)$ a 2nd-order LTI model identified on measured FRF data and $\mathcal{P}_{\text{act}}(s)$.

Next, the following information is employed: The minimum reference velocity is $\underline{v} = 0$. The following disturbances are acting on the system: Sensor noise η, modeled as white noise with zero mean and variance $\lambda_\eta^2 = (10^{-9})^2$; actuator noise $d_{i,\text{act}}$ modeled as white noise with zero mean and variance $\lambda_{d_{i,\text{act}}}^2 = (\sqrt{10^{-19}})^2$; periodic impact disturbances $d_{i,p}$ that depend on the reference velocity v, which are induced by piezoelectric actuators [21]; environmental disturbances $d_{o,\text{add}} = \mathcal{H}(s)\varepsilon$, where $\mathcal{H}(s)$ is depicted in Fig. 5 and ε is normally distributed white noise with zero mean and variance $\lambda_\varepsilon^2 = (2 \cdot 10^{-9})^2$. Furthermore, the performance measure is taken as the mean square of the error, which is given for an $N \times 1$ vector e by $e_{\text{MS}} := (1/N)\sum_{i=1}^{N} |e_i|^2$.

Next, a range of constant velocities $v_{c,i}$, $i = 1, 2, \ldots, 11$, are created in the set $v_{c,i} \in [0, \overline{v}]$, and 21 LTI controllers $\mathcal{C}_j(s)$ are designed each having a different bandwidth, $j = 1, 2, \ldots, 21$. These controllers all consist of the same types of linear filters, namely a lead filter, integrator, and second-order low-pass filter, and are given by

$$\mathcal{C}_j(s) = k_{p,j}\left\{\frac{s + 2\pi f_{I,j}}{s}\right\}\left\{\frac{\frac{1}{2\pi f_{le1,j}}s + 1}{\frac{1}{2\pi f_{le2,j}}s + 1}\right\} \times \left\{\frac{1}{\frac{1}{(2\pi f_{l,j})^2}s^2 + \frac{1}{2\pi f_{l,j}}s + 1}\right\} \tag{12}$$

where the parameters depend on the bandwidth $\omega_{b,j}$, are given by $f_{le1,j} = (1/4)\omega_{b,j}$, $f_{le2,j} = 4\omega_{b,j}$, $f_{I,j} = (1/9)\omega_{b,j}$ and $f_{l,j} = 6\omega_{b,j}$, with $j = 1, 2, \ldots, 21$. By shaping the gains $k_{p,j}$ to the appropriate value, 21 controllers with a different bandwidth $\omega_{b,j} \in [5, 25]$ Hz, $j = 1, 2, \ldots, 21$ have been designed. Then, following the procedure of **Step 1**, the performance as a function of the bandwidth for each $v_{c,i}$, $i = 1, 2, \ldots, 11$, is characterized and depicted in Fig. 6. This shows us that indeed the "optimal bandwidth" $\omega_{b,\text{opt},i}$ increases for increasing reference velocities $v_{c,i}$, $i = 1, 2, \ldots, 11$.

Step 2 in the Design: The LBW is chosen as $\underline{\omega}_b = 5$ Hz. The controller design of $\mathcal{C}_{\text{lbw}}(s)$ is based on the plant $\mathcal{P}_n(s)\mathcal{P}_{\text{act}}(s)$, thereby explicitly taking the hardware actuation filter $\mathcal{P}_{\text{act}}(s)$ into account. The hardware actuation filter has a cutoff frequency of 100 Hz, which does not pose limitations on achieving a bandwidth of $\underline{\omega}_b = 5$ Hz. However, $\mathcal{P}_{\text{act}}(s)$ does poses severe limitations on the maximum achievable bandwidth. Therefore, $\mathcal{P}_{\text{act}}(s)$ was *removed* from the setup

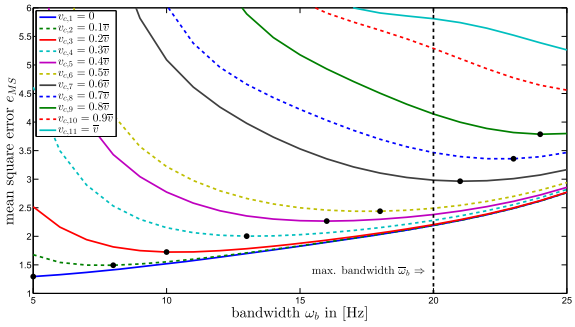

Fig. 6. Mean square of the closed-loop error e_{MS}, at various constant reference velocities $v_{c,i}$ as a function of the bandwidth ω_b. The black dots denote the minima of each curve, and thus the optimal bandwidth $\omega_{b,\text{opt},i}$ for each particular reference velocity, $i = 1, 2, \ldots, 11$.

and thus not included in the controller design of $\mathcal{C}_{\text{hbw}}(s)$, i.e., this is based on the plant $\mathcal{P}_n(s)$ only. In order to make a fair comparison with the LBW situation, an additional first-order low-pass filter $\mathcal{P}_{\text{act,hbw}}(s)$ is *digitally* included in the design of $\mathcal{C}_{\text{hbw}}(s)$. This filter $\mathcal{P}_{\text{act,hbw}}(s)$ is designed with cutoff frequency $20\overline{\omega}_b$ Hz, i.e., with the same ratio compared with the LBW (5 Hz) situation ($20\underline{\omega}_b = 100$ Hz). This finally results in an HBW controller $\mathcal{C}_{\text{hbw}}(s)$ that achieves a bandwidth of $\overline{\omega}_b = 20$ Hz.

Step 3 in the Design: In this step, we will first determine the shaping filter $\mathcal{F}_{\text{opt}}(s)$ and maximal gain $\bar{\alpha}_{\text{opt}}$ for the "optimal high-gain situation." Because the actuation filter $\mathcal{P}_{\text{act}}(s)$ will be present in the hardware during the experiments with the reference-dependent VGC $\mathcal{C}_{\text{vg}}$, we take this explicitly into account in the design of the shaping filter $\mathcal{F}_{\text{opt}}(s)$ (and later in $\mathcal{F}(s)$) in order to make a fair comparison with $\mathcal{C}_{\text{hbw}}(s)$ for high values of α. By doing so, the optimal gain $\bar{\alpha}_{\text{opt}}$ and optimal shaping filter $\mathcal{F}_{\text{opt}}(s)$ follow from:

$$\bar{\alpha}_{\text{opt}}\mathcal{F}_{\text{opt}}(s) = \frac{\mathcal{P}_{\text{act,hbw}}(s)\mathcal{C}_{\text{hbw}}(s)}{\mathcal{P}_{\text{act}}(s)\mathcal{C}_{\text{lbw}}(s)} - 1. \tag{13}$$

This results in a gain $\bar{\alpha}_{\text{opt}} = 129$ and a shaping filter $\mathcal{F}_{\text{opt}}(s)$ (which is normalized to gain 1 when $j\omega = 0$) as depicted in Fig. 7. It was already argued in Section III-B that this approach might result in a (too) high gain $\bar{\alpha}_{\text{opt}}$ such that satisfying the circle criterion condition of Theorem 4 is hard. Indeed, as indicated in Fig. 8, the solid green line intersects the green dashed line and, hence, we do not satisfy $Re(\mathcal{F}_{\text{opt}}(j\omega)\mathcal{T}(j\omega)) > -(1/129)$ for all $\omega \in \mathbb{R}$, for $\mathcal{T}(j\omega)$ as in (3) with $\mathcal{P}(j\omega) = \mathcal{P}_n(j\omega)\mathcal{P}_{\text{act}}(j\omega)$. Nevertheless, $\mathcal{F}_{\text{opt}}(s)$ forms a good starting point for the manual design of $\mathcal{F}(s)$. Closer inspection of Fig. 7 shows that the filter $\mathcal{F}(s)$ should have a -1 slope in the frequency range $\sim$ [0.7, 6] Hz, which basically represents the shift of the integrator to higher frequencies, which is realized by designing an appropriate lag filter. In the frequency range $\sim$ [30, 105] Hz, we observe a $+3$ slope in Fig. 7, which is realized by adding three lead filters. These create phase lead around the HBW by "canceling" the second-order low-pass filter in $\mathcal{C}_{\text{lbw}}(s)$ and the first-order low-pass actuation filter $\mathcal{P}_{\text{act}}(s)$ around those frequencies. Finally, in order to satisfy the circle criterion condition (8), a notch filter is added to fine-tune the shape of $\text{Re}(\mathcal{G}_{\text{eu}}(j\omega))$. This can

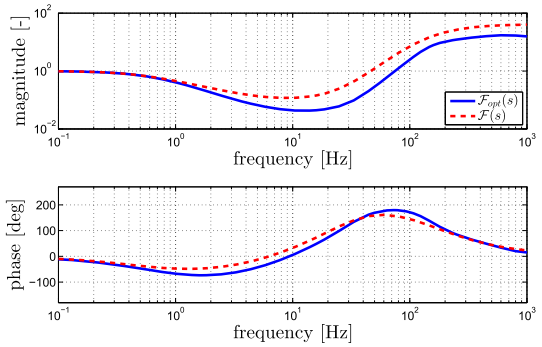

Fig. 7. Bode plot of the shaping filters $\mathcal{F}(s)$ and $\mathcal{F}_{\text{opt}}(s)$.

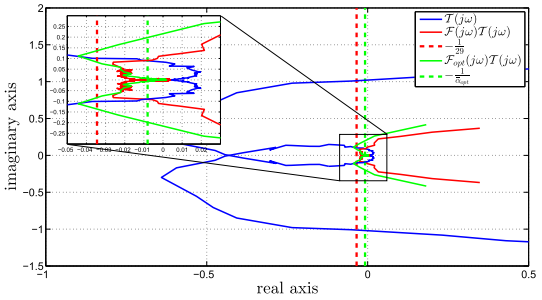

Fig. 8. Nyquist diagram for $\mathcal{G}_{\text{eu}}(j\omega)$ as in (3) for three cases. No shaping filter $\mathcal{F}(s)$ (blue solid curve), with shaping filter $\mathcal{F}(s)$ as in (14) (red solid curve), and with the optimal shaping filter $\mathcal{F}_{\text{opt}}(s)$ (green solid curve).

be done graphically by means of a Nyquist diagram of $\mathcal{G}_{\text{eu}}(j\omega)$ as in (3), with $\mathcal{P}(j\omega) = \mathcal{P}_n(j\omega)\mathcal{P}_{\text{act}}(j\omega)$. This tuning/loop-shaping procedure results in the shaping filter $\mathcal{F}(s)$ as depicted by the dashed line in Fig. 7, and which is given by the following transfer function:

$$\mathcal{F}(s) = \left\{\frac{\frac{1}{2\pi 26}s+1}{\frac{1}{2\pi 105}s+1}\right\}\left\{\frac{\frac{1}{2\pi 30}s+1}{\frac{1}{2\pi 110}s+1}\right\}^2\left\{\frac{\frac{1}{2\pi 6}s+1}{\frac{1}{2\pi 0.5}s+1}\right\} \times \left\{\frac{\frac{1}{(2\pi 26.5)^2}s^2+\frac{2\cdot 0.85}{2\pi 26.5}s+1}{\frac{1}{(2\pi 80)^2}s^2+\frac{2\cdot 1.3}{2\pi 80}s+1}\right\}. \quad (14)$$

Based on the circle criterion condition (8), the maximal gain is selected as $\bar{\alpha} = 29$, thereby allowing for some robustness margin (see Fig. 8) which shows that the solid red line stays on the right of the red dashed line with some margin. Once the circle criterion condition (8) has been verified, i.e., $Re(\mathcal{G}_{\text{eu}}(j\omega)) > -(1/29)$ for all $\omega \in \mathbb{R}$, and realizing that $\mathcal{G}_{\text{eu}}(j\omega) \to 0$ for $\omega \to \infty$, condition (II) of Theorem 4 is satisfied. In order to verify condition (I), note that the LBW controller $\mathcal{C}_{\text{lbw}}(s)$ is designed such that the open-loop $\mathcal{P}_n(s)\mathcal{P}_{\text{act}}(s)\mathcal{C}_{\text{lbw}}(s)$ satisfies the Nyquist stability criterion [14]. Since the shaping filter $\mathcal{F}(s)$ as in (14) has no unstable poles, we also satisfy condition (I) of Theorem 4 (see Remark 5). Hence, we can conclude that all conditions of Theorem 4 are being satisfied, which guarantees that the designed reference-dependent VGC system is exponentially convergent, independent of how the gain $\alpha(v(t)) \in [0, 29]$, $t \in \mathbb{R}_{\geq 0}$, varies over time.

Step 4 in the Design: The mapping $\alpha : [0, \overline{v}] \to [0, 29]$ is obtained by following the three design parts listed in **Step 4**.

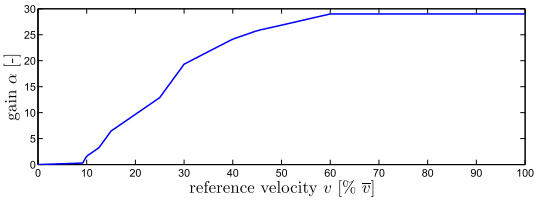

Fig. 9. Designed "reference-to-gain" mapping.

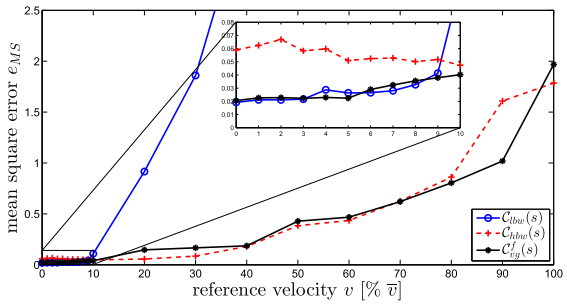

Fig. 10. Performance measure of the measured steady-state error e of the nanomotion stage during 20 constant velocities v_c in the range $[0, \overline{v}]$ (represented in % of $\overline{v}$).

The "reference-to-gain" mapping $\alpha : [0, \overline{v}] \to [0, 29]$ that is used during the experiments is depicted in Fig. 9.

C. Experimental Results

Let us start with presenting the results of the performance analysis of the measured steady-state error e, depicted in Fig. 10. The analysis is performed for constant reference velocities $v(t) = v_c$, for all $t \in \mathbb{R}_{\geq 0}$, using the two linear controllers $\mathcal{C}_{\text{lbw}}(s)$ and $\mathcal{C}_{\text{hbw}}(s)$ and the reference-dependent VGC $\mathcal{C}^f_{\text{vg}}(s)$ as in (1) for different *fixed* values of $\alpha \in [0, 29]$. Note that for each velocity v_c, there exists a corresponding $\alpha \in [0, 29]$ (see Fig. 9). Let us first focus on low velocities v_c in the range $[0, 0.1 \cdot \overline{v}]$, see the zoom plot in Fig. 10. Clearly, in this range, both the LBW controller $\mathcal{C}_{\text{lbw}}(s)$ as well as the reference-dependent VGC $\mathcal{C}^f_{\text{vg}}(s)$ perform better than the HBW controller $\mathcal{C}_{\text{hbw}}(s)$ as their mean-square error e_{MS} is significantly lower (at $v_c = 0$) or, at worst, (approximately) equal (at $v_c = 0.1 \cdot \overline{v}$). At standstill, we achieve (approximately) the same performance with the VGC $\mathcal{C}^f_{\text{vg}}(s)$ (with $\alpha = 0$) as for $\mathcal{C}_{\text{lbw}}(s)$, while compared with $\mathcal{C}_{\text{hbw}}(s)$, the performance is increased by $\sim 66\%$. This is due to the fact that for this case, the disturbances $d_{o,\text{add}}$, $d_{i,a}$ and η are being dominant, which are more amplified in the HBW situation. The increase in performance compared with the HBW situation is also clearly visible in the time-domain (see Fig. 11), which shows the measured steady-state error at standstill.

Fig. 10 also shows that the higher the reference velocity v_c, the more beneficial it is to have a higher bandwidth controller. This is due to the fact that for increasing reference velocities, the periodic disturbance d_p due to the piezoelectric actuator becomes more influential and eventually dominant over $d_{o,\text{add}}$, $d_{i,a}$, and η. The effect of this disturbance is suppressed by increasing the gain α, and as a result, the "bandwidth" ω_b of the VGC $\mathcal{C}_{\text{vg}}$. With this in mind, let us now focus in Fig. 10 on the velocities v_c in the range $[0.1 \cdot \overline{v}, \overline{v}]$. As expected, the LBW

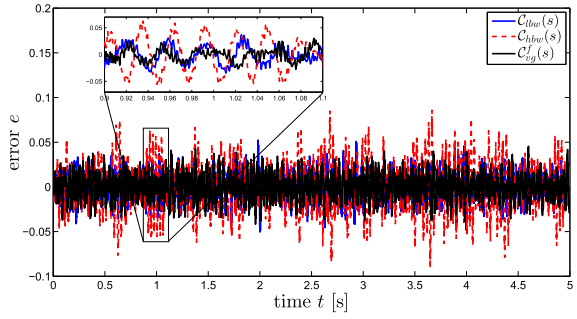

Fig. 11. Measured steady-state error e of the nanomotion stage during standstill, i.e., velocity $v_c = 0$.

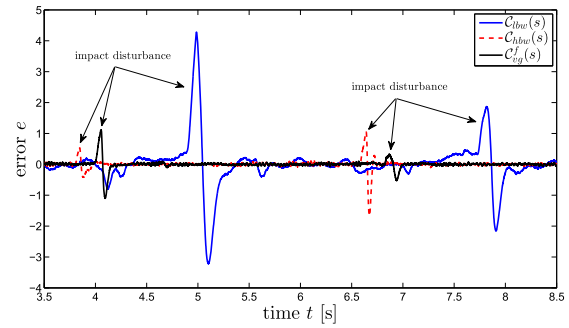

Fig. 12. Measured steady-state error e of the nanomotion stage during a constant velocity $v_c = \overline{v}$.

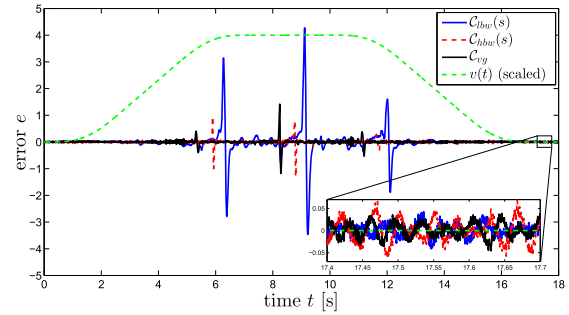

Fig. 13. Time-domain performance analysis, moving from $v(t) = 0$ to $v(t) = \overline{v}$ with a constant acceleration, and back to $v(t) = 0$.

controller $\mathcal{C}_{\text{lbw}}(s)$ performs worst, since its bandwidth of 5 Hz is too low to suppress the periodic impact disturbances d_p. The HBW controller $\mathcal{C}_{\text{hbw}}(s)$ and our reference-dependent VGC $\mathcal{C}_{\text{vg}}^{f}(s)$ show an approximately similar performance, which is superior compared with that of $\mathcal{C}_{\text{lbw}}(s)$.

Fig. 12 shows the measured steady-state error at a high constant velocity of $\overline{v}$ for which the low-frequency periodic disturbance d_p is dominant. The performance of the HBW controller $\mathcal{C}_{\text{hbw}}(s)$ and the VGC $\mathcal{C}_{\text{vg}}^{f}(s)$ are comparable, as was already indicated in Fig. 10. It is clear that the periodic impact disturbances d_p are much better suppressed by $\mathcal{C}_{\text{hbw}}(s)$ and $\mathcal{C}_{\text{vg}}^{f}(s)$ than using the LBW controller $\mathcal{C}_{\text{lbw}}(s)$.

The previous results were obtained for constant reference velocities, resulting in fixed values of α and, hence, a comparison between $\mathcal{C}_{\text{lbw}}(s)$ and $\mathcal{C}_{\text{hbw}}(s)$ with a linear controller $\mathcal{C}_{\text{vg}}^{f}(s)$. However, it is (also) important to compare the behavior for *time-varying* velocity profiles, which is depicted in Fig. 13. Fig. 13 shows the time-domain error behavior for a constant acceleration, starting from $v(t) = 0$ until we move at $v(t) = \overline{v}$ for approximately 5 s, and then moving back to $v(t) = 0$. Indeed, as indicated in Fig. 13, the performance using $\mathcal{C}_{\text{vg}}$ for low velocities is comparable with using $\mathcal{C}_{\text{lbw}}(s)$, while for high velocities, the performance of $\mathcal{C}_{\text{vg}}$ is similar to $\mathcal{C}_{\text{hbw}}(s)$. This demonstrates that the proposed reference-dependent VGC $\mathcal{C}_{\text{vg}}$ is able to deal with reference-dependent conflicting control design tradeoffs. In fact, the experiments show that the VGC $\mathcal{C}_{\text{vg}}$ can achieve "the best of both worlds," referring to preferring a controller that results in an LBW $\underline{\omega}_b$ over a controller that results in an HBW $\overline{\omega}_b$, or vice versa, depending on the actual reference information.

V. Conclusion

In this brief, we proposed a novel reference-dependent VGC strategy that allows for a varying "bandwidth" of the feedback controller. A complete design framework for such reference-dependent VGCs has been presented, in which most of the design steps involve the usage of state-of-practice frequency-domain loop-shaping tools. This design feature, together with graphical data-based conditions to verify stability and convergence of the VGC closed-loop system, makes the analysis and design intuitive for control engineers and, as such, connects to the industrial control engineering practice. The design framework has been illustrated based on an industrial nanopositioning motion stage with challenging and conflicting linear control goals. It has been experimentally demonstrated that the proposed reference-dependent VGC indeed has the ability to outperform (fixed bandwidth) LTI controllers.

References

[1] M. Seron, J. Braslavsky, and G. Goodwin, *Fundamental Limitations in Filtering and Control*. Berlin, Germany: Springer, 1997.

[2] M. Steinbuch and M. L. Norg, "Advanced motion control: An industrial perspective," *Eur. J. Control*, vol. 4, no. 4, pp. 278–293, 1998.

[3] B. G. B. Hunnekens, M. F. Heertjes, N. van de Wouw, and H. Nijmeijer, "Performance optimization of piecewise affine variable-gain controllers for linear motion systems," *Mechatronics*, vol. 24, no. 6, pp. 648–660, 2014.

[4] J. Zheng, G. Guo, and Y. Wang, "Nonlinear PID control of linear plants for improved disturbance rejection," in *Proc. 16th IFAC World Congr.*, vol. 16. 2005, pp. 281–286.

[5] N. van de Wouw, H. A. Pastink, M. F. Heertjes, A. V. Pavlov, and H. Nijmeijer, "Performance of convergence-based variable-gain control of optical storage drives," *Automatica*, vol. 44, no. 1, pp. 15–27, 2008.

[6] M. F. Heertjes and H. Nijmeijer, "Self-tuning of a switching controller for scanning motion systems," *Mechatronics*, vol. 22, no. 3, pp. 310–319, 2012.

[7] B. Armstrong, D. Neevel, and T. Kusik, "New results in NPID control: Tracking, integral control, friction compensation and experimental results," *IEEE Trans. Control Syst. Technol.*, vol. 9, no. 2, pp. 399–406, Mar. 2001.

[8] M. Dinh, G. Scorletti, V. Fromion, and E. Magarotto, "Parameter dependent H_∞ control by finite dimensional LMI optimization: Application to trade-off dependent control," *Int. J. Robust Nonlinear Control*, vol. 15, no. 9, pp. 383–406, 2005.

[9] J. S. Shamma and M. Athans, "Guaranteed properties of gain scheduled control for linear parameter-varying plants," *Automatica*, vol. 27, no. 3, pp. 559–564, 1991.

[10] C. W. Scherer, "LPV control and full block multipliers," *Automatica*, vol. 37, no. 3, pp. 361–375, 2001.
[11] K. S. Narendra and J. Balakrishnan, "Adaptive control using multiple models," *IEEE Trans. Autom. Control*, vol. 42, no. 2, pp. 171–187, Feb. 1997.
[12] D. Liberzon, *Switching in Systems and Control*, Boston, MA, USA: Birkhäuser Verlag, 2003.
[13] W. P. M. H. Heemels, B. D. Schutter, J. Lunze, and M. Lazar, "Stability analysis and controller synthesis for hybrid dynamical systems," *Philos. Trans. Roy. Soc. London A, Math. Phys. Sci.*, vol. 368, no. 1930, pp. 4937–4960, 2010.
[14] S. Skogestad and I. Postlethwaite, *Multivariable Feedback Control: Analysis and Design*. Hoboken, NJ, USA: Wiley, 2005.
[15] B. P. Demidovich, "Dissipativity of a nonlinear system of differential equations, Part I," *Ser. Mat. Mekh.*, vol. 6, pp. 19–27, 1961.
[16] A. Pavlov, N. van de Wouw, and H. Nijmeijer, *Uniform Output Regulation of Nonlinear Systems: A Convergent Dynamics Approach*. Boston, MA, USA: Birkhäuser Verlag, 2006.
[17] H. K. Khalil, *Nonlinear Systems*. Englewood Cliffs, NJ, USA: Prentice-Hall, 2000.
[18] J. P. Hespanha, *Linear Systems Theory*. Princeton, NJ, USA: Princeton Univ. Press, 2009.
[19] V. A. Yakubovich, "The matrix inequalities method in the theory of the stability of nonlinear control systems - I," *Autom. Remote Control*, vol. 7, pp. 905–917, 1964.
[20] S. Devasia, E. Eleftheriou, and S. O. R. Moheimani, "A survey of control issues in nanopositioning," *IEEE Trans. Control Syst. Technol.*, vol. 15, no. 5, pp. 802–823, Sep. 2007.
[21] R. Merry, "Performance-driven control of nano-motion systems," Ph.D. dissertation, Dept. Mech. Eng., Eindhoven Univ. Technol., Eindhoven, The Netherlands 2009.